

Muon-Induced Background Study for an Argon-Based Long Baseline Neutrino Experiment

D. Barker,¹ D.-M. Mei,^{1,*} and C. Zhang^{1,2}

¹ *Department of Physics, The University of South Dakota, Vermillion, South Dakota 57069*

² *College of Sciences, China Three Gorges University, Yichang 443002, China*

We evaluated rates of transversing muons, muon-induced fast neutrons, and production of ^{40}Cl and other cosmogenically produced nuclei that pose as potential sources of background to the physics program proposed for an argon-based long baseline neutrino experiment at the Sanford Underground Research Facility (SURF). The Geant4 simulations were carried out with muons and muon-induced neutrons for both 800 ft (0.712 km.w.e.) and 4850 ft levels (4.3 km.w.e.). We developed analytic models to independently calculate the ^{40}Cl production using the measured muon fluxes at different levels of the Homestake mine. The muon induced ^{40}Cl production rates through stopped muon capture and the muon-induced neutrons and protons via (n,p) and (p,n) reactions were evaluated. We find that the Monte Carlo simulated production rates of ^{40}Cl agree well with the predictions from analytic models. A depth-dependent parametrization was developed and benchmarked to the direct analytic models. We conclude that the muon-induced processes will result in large backgrounds to the physics proposed for an argon-based long baseline neutrino experiment at a depth of less than 4.0 km.w.e.

PACS numbers: 13.85.Hd, 23.40.-s, 25.40.Fq

I. INTRODUCTION

Experiments for the past several decades require modification of the Standard Model to incorporate the unexpected neutrino properties and fundamental characteristics [1–8]. For instance, neutrino flavor mixing was found to be responsible for the phenomenon of neutrino oscillation [1–8] occurring between three generations in which a complex phase (δ_{CP}) signifies the amount of violation of the charge-parity (CP) symmetry, which is unknown. The value of the mixing angle, θ_{13} , between the first generation and the third generation, is also unknown, but an upper limit of $<10^\circ$ is given by CHOOZ experiment [9] at the 90% C.L. The sign of the mass difference, Δm_{13}^2 , which represents the ordering of the mass eigenstates, remains unknown as well. These three unknown parameters are intended to be addressed with the next generation of neutrino oscillation experiments.

Recent studies of neutrino properties using neutrino beams have demonstrated that good sensitivity to CP violation and the mass hierarchy can be achieved by measuring ν_e appearance using a very long baseline ν_μ beam with massive detectors [10] assuming the value of $\theta_{13} > 1^\circ$. The recent values of θ_{13} measured by MINOS and T2K shows a non-zero value [11, 12] that is particularly interesting to the measurements of CP violation and mass hierarchy. The proof of CP violation in the lepton sector and the knowledge of the value of δ_{CP} are crucial to understanding the origin of the baryon asymmetry in the universe, providing a strong implication of leptogenesis that is responsible for the observed baryon asymmetry of

the universe [13]. Simultaneously, the neutrino mass hierarchy is of great importance for neutrinoless double-beta decay experiments [14] and could shed light on possible flavor symmetries.

When measuring the value of θ_{13} , CP phase, δ_{CP} , and the neutrino mass hierarchy with conventional neutrino beams, a key process of new discovery in neutrino oscillation is $\nu_\mu \rightarrow \nu_e$ appearance. With appropriate detector design and adequate control of environmental factors, specifically proper shielding, the long baseline neutrino experiment (LBNE) [15, 16] is capable of supporting an extremely rich program of high energy physics and particle-astronomy including proton decay, astronomical neutrinos, and tests of fundamental physics and the Standard Model. The two detector technologies being considered are: 1) an active finely grained liquid argon time-projection-chamber (LAr-TPC) and 2) a water Cerenkov detector. Both detector technologies can support this wide range of physics goals probing the Standard Model and searching for physics beyond the current models. However, muon-induced background may constrain the sensitivity of the proposed experiment, in particular, the proposed galactic and relic supernova neutrino detection with liquid argon detector. Though the background can be measured for beam neutrino physics with the beam-on or -off, the fluctuation of background events can be problematic if these events occur on the same order of magnitude as anticipated physics signal. In addition to the beam contamination backgrounds, the main sources are the muon-induced processes. In this paper, we report the study of the muon-induced backgrounds for an argon-based detector.

Muons and muon-induced fast neutrons entering the detector from the surrounding rock can result in troublesome experimental backgrounds. While through-going muon events in the detector have energy depositions and

*Corresponding Author: Department of Physics, The University of South Dakota, Vermillion, South Dakota 57069

can be easily identified, muons that traverse the rock near the detector, or traverse very small distances in the detector ("corner-clippers"), can result in limiting backgrounds. Moreover, background events can be produced by the muon-induced fast neutrons entering the detector while the parent muons pass completely through the surrounding in-active materials. The muon-induced neutrons can undergo (n,p) reaction with ^{40}Ar , and negative muons capture on ^{40}Ar . Both reactions create unwanted ^{40}Cl , which can be a background for the following reactions: $\bar{\nu}_e + ^{40}\text{Ar} \rightarrow e^- + ^{40}\text{Cl}$, $\nu_e + ^{40}\text{Ar} \rightarrow e^- + ^{40}\text{K}$, $\nu_x + ^{40}\text{Ar} \rightarrow \nu_x + ^{40}\text{Ar}^*$, and $\nu_{x,\bar{x}} + e^- \rightarrow \nu_x + e^-$, where $x = e, \mu, \tau$. This is because the decay Q value of ^{40}Cl is 7.48 MeV which is above the proposed detection threshold of 5 MeV or 6 MeV, and the half-life of ^{40}Cl is 1.35 minutes making it difficult to correlate with muons. There can also be additional radioactive isotopes produced by muon-induced processes in the argon target. Those radioactive isotopes can be part of the background for the proposed physics channels. Therefore, it is necessary to evaluate the muon-induced processes and the production rate of the cosmogenics in the detector volume.

Due to the lack of direct detection measurements of the muons and muon-induced products and parameters for a given depth with a given detector, such an evaluation has not been modelled in full. In this paper, we present several parametrization functions that estimate the muon-induced fast neutron energy spectrum and the stopping muons as a function of depth. Using these parametrization functions, we simulated cosmogenic production rates in the proposed LBNE LAr detector for two depths with a well known Geant4 package [18], Geant4.9.5 with shielding physics list. The simulated results were compared to the predictions by the developed analytic models. Since the muon-induced processes are strongly depth dependent [17], we establish a depth-sensitivity relation for an argon-based detector by calculating the production rates of muon-induced processes as a function of depth.

II. EVALUATION OF MUON-INDUCED BACKGROUND

At sufficiently high energies, radiative processes become predominant in energy loss for muons. Many sub-sequential particles can be produced by muon-induced radiative processes. Cosmogenic radioactive isotopes can be produced by muons and muon-induced sequential particles including neutrons, protons, pions, gamma rays, etc. Two cases are considered in the following evaluation: 1) muons transversing the detector and 2) muon-induced neutrons entering the detector from the experimental hall. The former process creates ^{40}Cl and other radioactive isotopes through negative muon capture, (n,p) reaction, and (p,n) reaction, etc. The latter produces backgrounds mainly through high energy events, π_0 and ^{40}Cl productions. In order to understand the production rates and their corresponding mechanisms, we performed a full

Geant4 Monte Carlo simulation and developed analytic models. We elaborate on the evaluation processes in the following subsections.

A. Muon-induced Background from the Geant4 Simulation

High energy cosmic-ray muons can penetrate rock overburden to reach an underground laboratory with the surviving muons generating neutrons in the surrounding rock. Those neutrons are unwanted particles that could produce background events for low-background experiments searching for rare event physics. The intensities of the residual muons and the muon-induced neutrons depend strongly on the depth of the underground detector. This is particularly important for detecting supernova neutrinos that contribute to a signal range of a few MeV to a few tens of MeV, which can often be dominated by the muon-induced backgrounds depending on the depth. Therefore, the depth-sensitivity relation needs to be understood in order to choose an appropriate depth at the Sanford Underground Research Facility (SURF) to estimate the experimental limitations imposed by these backgrounds and to optimize the detector design for the full range of possible physics programs. Because both the 800-ft level and the 4850-ft level are being considered for a far detector, we have conducted Geant4 Monte Carlo simulations to understand the cosmogenic production in the detector at both levels.

In the Geant4 simulation, a simple geometry with a dimension of liquid argon, 45.6 m (width) \times 22.4 m (length) \times 14.0 m (height) [15], was placed in a stainless steel container with a thickness of 1 cm. Both muons and neutrons were generated on a very thin sheet (100 m (width) \times 50 m (length)) right above the upper surface of the stainless steel tank. Since the thin sheet is two times larger than the size of the detector in length and width, both muons and neutrons generated in the sheet can enter the detector with angular distribution of $\sec(\theta)$. There is a wide range of thetas that are enabled by taking a large production sheet and better represent the range of anticipated underground muons. Note that we assume the parent muons and daughter neutrons have the same angular distribution. The residual muon energy spectrum was obtained from equation (8) of Ref. [17]. The normalization constant was determined using equation (4) in Ref. [17]. The muon-induced neutron energy spectrum was given in equation (14) in Ref. [17]. However, this equation cannot be directly used to generate neutrons for a given depth without knowing the associated parameters. We adopt the following procedures to obtain the neutron energy spectrum as a function of depth. First, the average neutron energy as a function of depth was studied using the simulated results for various depths in Tables I and VII from Ref. [17] and a measured surface data point from Ref. [19]. Fig. 1 shows the fitted curve.

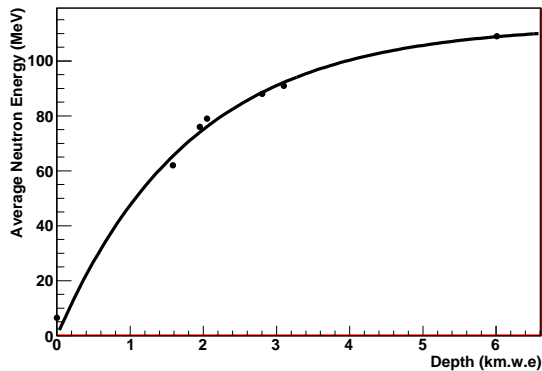


FIG. 1: Average neutron energy as a function of depth.

The fitted function can be expressed as

$$\langle E_n \rangle = 113 \cdot [1 - \exp(-0.545 \cdot h)], \quad (1)$$

where h is the depth in km.w.e. At 800 ft, $\langle E_n \rangle$ is 36.3 MeV, and at 4850 ft, $\langle E_n \rangle$ is 102.2 MeV. It is noticed that the average neutron energy at the depth of Gran Sasso is about 91 MeV [17]. This is not much different from the average neutron energy predicted for the 4850-ft level at Homestake. This is because the production mechanisms are primarily sensitive to the overburden of rock and do not depend much on site specific details. Therefore, we then used the parameters in Table VII of Ref. [17] to generate neutrons for the depth of Gran Sasso. The normalization is done with equation (13) in Ref. [17] that predicts the muon-induced neutron flux as a function of depth for depths greater than 1.6 km.w.e. One caveat in this method is the ignorance of rock composition, which could make a difference of up to about 35% [17]. The muon-induced neutron energy spectrum at the 800-ft level was obtained using a scaling method. We scaled the neutron energy spectrum from the depth of 4850 ft to the depth of the 800 ft using a scaling factor, $(\frac{\langle E_{\mu,800} \rangle}{\langle E_{\mu,4850} \rangle})^\alpha \frac{\Phi_{\mu,800}}{\Phi_{\mu,4850}}$, where $\langle E_{\mu,800} \rangle$, $\Phi_{\mu,800}$, and $\langle E_{\mu,4850} \rangle$, $\Phi_{\mu,4850}$, are the average muon energies and the total muon fluxes for the 800-ft level and the 4850-ft level at Homestake, respectively. $\alpha = 0.73$ is a constant. Note that the primary concerns of the cosmogenic production are ^{40}Cl and ^{40}K through negative muon capture, (n,p), and (p,n) reactions. Since the reaction threshold of $^{40}\text{Ar}(n,p)^{40}\text{Cl}$ requires neutrons with kinetic energy greater than 6.87 MeV, this cuts the majority of neutrons induced by natural radioactivity in rock through (α,n) reactions. Therefore, we neglected the calculation of ^{40}Cl production by (α,n) neutrons.

1. Muon-induced Background at the 800-ft Level

The muons that survived the 800-ft rock at Homestake have an average energy of ~ 97 GeV and a flux of

$6.3 \times 10^{-6} \text{cm}^{-2} \text{s}^{-1}$ from equation (9) and equation (4) in Ref. [17]. These high energy muons passing through the surrounding rock of a laboratory will generate fast neutrons. The emerging neutrons in an experimental hall have an average energy of ~ 36 MeV with a total flux of $3.2 \times 10^{-7} \text{cm}^{-2} \text{s}^{-1}$. The neutron energy spectrum obtained from the methods described above is shown in Fig. 2. We simulated the muons passing through the de-

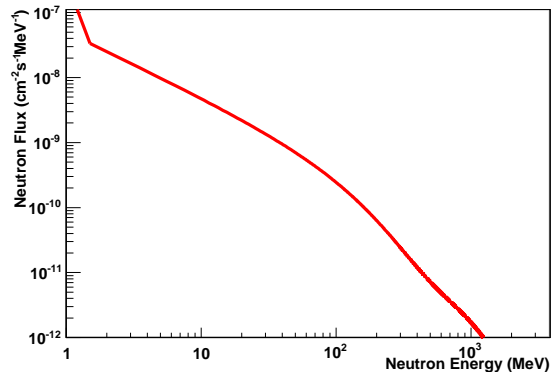


FIG. 2: Local fast neutron energy spectrum at the 800-ft level used in the Monte Carlo simulation.

tector and the muon-induced neutrons entering the detector from rock. Fig. 3 shows a visible energy spectrum induced by the muon-induced neutrons entering the detector from the surrounding rock. The event rate above 5 MeV in a 20 kton detector is ~ 0.28 Hz. The direct muon rate is ~ 88 Hz. These rates are high enough to potentially swamp any signals from a galactic supernova (~ 44 Hz estimated using Ref. [20]) or even from a neutrino beam (~ 75 events per year for ν_e appearance estimated with Ref. [21]).

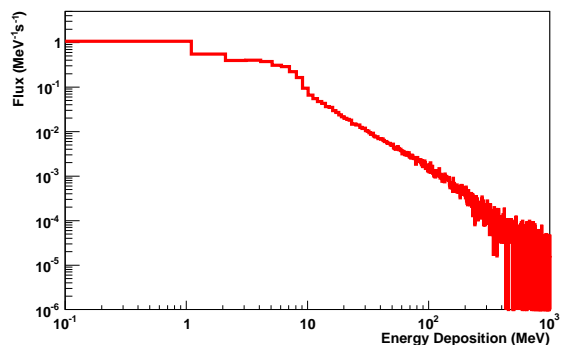


FIG. 3: Fast neutrons induced visible energy spectrum in the detector at the 800-ft level. A flat ionization efficiency of 25% was applied to the nuclear recoil events in this plot.

We summarize the ^{40}Cl production rates from the above two sources in Table I. It is also interesting to show the overall cosmogenic production in the detector. As shown in Table II and Fig. 4, the cosmogenic isotopes

TABLE I: ^{40}Cl production rates in the detector (20 kton) at the 800-ft level.

| From μ simulation | | From n simulation | |
|-----------------------|--------------|---------------------|--------------|
| Produced by | Rate per day | Produced by | Rate per day |
| Muon Capture | 27344 | Secondary μ | 45 |
| Secondary n | 40587 | Neutrons | 3667 |
| Pions | 249 | Pions | 1.4 |
| Others | 83 | Others | < 1 |
| Total | 68163 | Total | 3714 |

induced by muons range from P to Ca, a total rate of 19 Hz. Some of them can be background to the proposed physics channels.

TABLE II: Additional significant cosmogenic production rates in the detector (20 kton) at the 800-ft level.

| Isotope | Produced by | Rate per day | Q (MeV) | $t_{1/2}$ |
|------------------|----------------|--------------|---------|----------------------|
| ^{30}P | Spallation | 9020 | 4.23 | 2.5 m |
| ^{32}P | Spallation | 20900 | 1.71 | 14. 3 d |
| ^{33}P | Spallation | 30100 | 0.25 | 25.3 d |
| ^{34}P | Spallation | 12090 | 5.4 | 12.4 s |
| ^{35}P | Spallation | 7500 | 4.0 | 47. 2 s |
| ^{36}P | Spallation | 1190 | 10.4 | 5.6 s |
| ^{37}P | Spallation | 550 | 7.9 | 2.3 s |
| ^{31}S | Spallation | 5500 | 5.4 | 2.6 s |
| ^{35}S | Spallation | 215500 | 0.17 | 87.5s |
| ^{37}S | (n, α) | 31500 | 4.9 | 5.1 m |
| ^{38}S | Spallation | 11500 | 2.9 | 170 m |
| ^{39}S | Spallation | 850 | 6.6 | 11.5 s |
| ^{33}Cl | Spallation | 670 | 5.6 | 2.5 s |
| ^{34}Cl | Spallation | 8700 | 5.6 | 32 m |
| ^{36}Cl | Spallation | 1005000 | 0.7 | 3.1×10^5 y |
| ^{38}Cl | Spallation | 110000 | 4.9 | 37.24 m |
| ^{35}Ar | (n, $6n'$) | 7100 | 6.0 | 1.8 s |
| ^{37}Ar | (n, $4n'$) | 21000 | 0.8 | 35 d |
| ^{39}Ar | (n, $2n'$) | 91000 | 0.57 | 269 y |
| ^{41}Ar | capture | 45100 | 2.5 | 109 m |
| ^{38}K | Spallation | 650 | 5.9 | 7.6 m |
| ^{40}K | (p,n) | 6500 | 1.3 | 1.28×10^9 y |
| Total | | 1641920 | | |

2. Cosmogenic Production at the 4850-ft Level

The residual muons at the 4850-ft level have an average of ~ 321 GeV using the equation (9) in Ref. [17]. The total flux is predicted to be $4.4 \times 10^{-9} \text{cm}^{-2} \text{s}^{-1}$ in Ref. [17]. The neutrons that are produced in the rock by these residual high energy muons entering the experimental hall were simulated by Mei & Hime in great detail [17]. We obtained a muon-induced neutron energy spectrum using the method described in Section II A. Fig. 5 shows the neutron energy spectrum. The total flux at the 4850-ft level is $5.4 \times 10^{-10} \text{cm}^{-2} \text{s}^{-1}$. The production of ^{40}Cl is via (n,p) reaction on ^{40}Ar requiring a threshold of 6.87 MeV. The total neutron flux with neutron energy greater

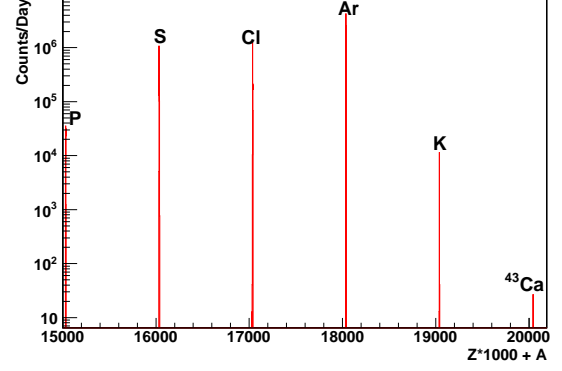


FIG. 4: Muon-induced cosmogenic production at the 800-ft level.

than 6.87 MeV is about $1.6 \times 10^{-10} \text{cm}^{-2} \text{s}^{-1}$.

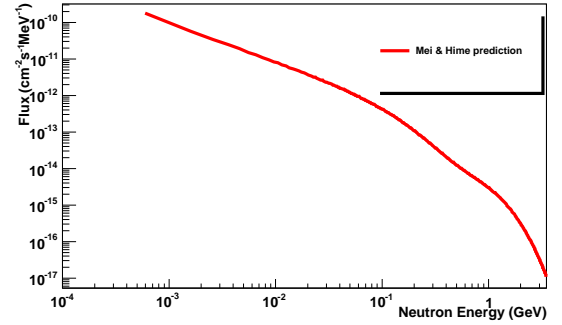


FIG. 5: Local fast neutron energy spectrum used in the Monte Carlo simulation.

Similar to the simulation for the 800-ft level, we simulated both the residual muons crossing the detector and the muon-induced neutrons entering the detector from rock. The visible energy spectrum induced by the muon-induced neutrons entering the detector from the surrounding rock is shown in Fig. 6. The event rate above 5 MeV is ~ 0.001 Hz. The direct muon rate is ~ 0.05 Hz.

Table III shows the simulated ^{40}Cl production rates from two sources.

TABLE III: ^{40}Cl production rates in the detector (20 kton) at the 4850-ft level.

| From μ simulation | | From n simulation | |
|-----------------------|--------------|---------------------|--------------|
| Produced by | Rate per day | Produced by | Rate per day |
| Muon Capture | 17.5 | Secondary μ | 0.43 |
| Secondary n | 54.4 | Neutrons | 9.3 |
| Pions | 0.33 | Pions | 0.016 |
| Others | 0.04 | Others | 0.002 |
| Total | 72.3 | Total | 8.41 |

Similar to the above discussion of the cosmogenic production for the 800-ft level, we show overall cosmogenic

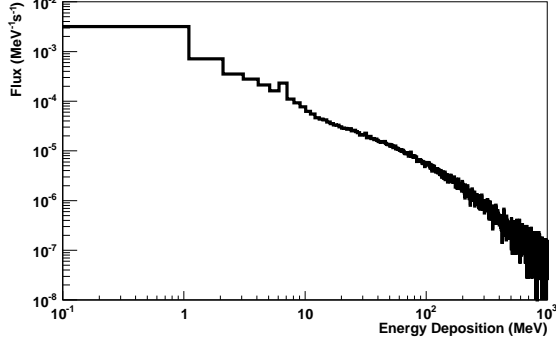


FIG. 6: Fast neutrons induced visible energy spectrum in the detector at the 4850-ft level. A flat ionization efficiency of 25% was applied to the nuclear recoil events in this plot.

isotopes induced by muons for the 4850-ft level in Table IV and Fig. 7. Note that the production rate is relatively small at this depth.

TABLE IV: Additional significant cosmogenic production rates in the detector (20 kton) at the 4850-ft level.

| Isotope | Produced by | Rate per day | Q (MeV) | $t_{1/2}$ |
|------------------|----------------|--------------|---------|----------------------|
| ^{30}P | Spallation | 9.6 | 4.23 | 2.5 m |
| ^{32}P | Spallation | 22.2 | 1.71 | 14. 3 d |
| ^{33}P | Spallation | 31.9 | 0.25 | 25.3 d |
| ^{34}P | Spallation | 12.8 | 5.4 | 12.4 s |
| ^{35}P | Spallation | 8.0 | 4.0 | 47. 2 s |
| ^{36}P | Spallation | 1.3 | 10.4 | 5.6 s |
| ^{37}P | Spallation | 0.6 | 7.9 | 2.3 s |
| ^{31}S | Spallation | 5.8 | 5.4 | 2.6 s |
| ^{35}S | Spallation | 228.5 | 0.17 | 87.5s |
| ^{37}S | (n, α) | 33.4 | 4.9 | 5.1 m |
| ^{38}S | Spallation | 12.2 | 2.9 | 170 m |
| ^{39}S | Spallation | 0.9 | 6.6 | 11.5 s |
| ^{33}Cl | Spallation | 0.7 | 5.6 | 2.5 s |
| ^{34}Cl | Spallation | 9.2 | 5.6 | 32 m |
| ^{36}Cl | Spallation | 1065.7 | 0.7 | 3.1×10^5 y |
| ^{38}Cl | Spallation | 116.6 | 4.9 | 37.24 m |
| ^{35}Ar | (n, $6n'$) | 7.5 | 6.0 | 1.8 s |
| ^{37}Ar | (n, $4n'$) | 22.3 | 0.8 | 35 d |
| ^{39}Ar | (n, $2n'$) | 96.5 | 0.57 | 269 y |
| ^{41}Ar | capture | 47.8 | 2.5 | 109 m |
| ^{38}K | Spallation | 0.69 | 5.9 | 7.6 m |
| ^{40}K | (p,n) | 6.9 | 1.3 | 1.28×10^9 y |
| Total | | 1741 | | |

B. Development of Analytic Models

It is of general interest to have analytic models that can be used to estimate the cosmogenic production rates without doing a complicated simulation procedure. Even after a campaign of Monte Carlo simulation, it is necessary to assess whether a correct result was delivered by

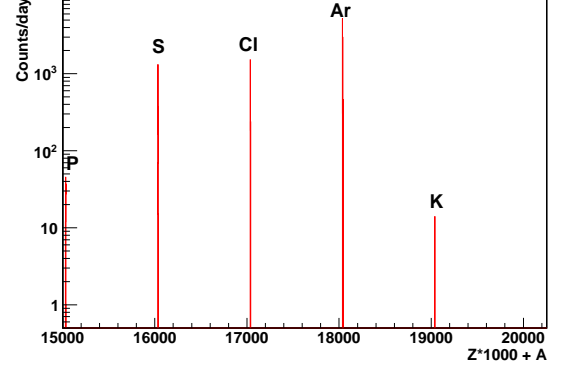


FIG. 7: Muon-induced cosmogenic production at the 4850-ft level.

a complicated simulation package. Analytic models are developed based on the physics processes that are then compared to the experimental results. Therefore, analytic models can be used to compare and evaluate the results from a full Monte Carlo simulation. We develop analytic models below.

1. Solid Angle

When considering the interaction of particles in a detector, it is necessary to calculate the solid angle subtended a certain distance from the target. Using the work of H. Gotoh and H. Yagi [22], the solid angle of a point particle was calculated at an arbitrary distance from the detector as well as the subtended solid angle from a fixed point throughout the detector material. For an assumed LBNE detector of dimensions ($2w \times 2l \times h$) = $(45.6 \times 22.4 \times 14)$ m³, the solid angle from a point (x_p, y_p, z_p) is

$$\begin{aligned}
 \Omega = & \arctan \frac{(x_p + w)(y_p + l)}{z_p((x_p + w)^2 + (y_p + l)^2 + z_p^2)^{1/2}} \\
 & - \arctan \frac{(x_p + w)(y_p - l)}{z_p((x_p + w)^2 + (y_p - l)^2 + z_p^2)^{1/2}} \\
 & - \arctan \frac{(x_p - w)(y_p + l)}{z_p((x_p - w)^2 + (y_p + l)^2 + z_p^2)^{1/2}} \\
 & + \arctan \frac{(x_p - w)(y_p - l)}{z_p((x_p - w)^2 + (y_p - l)^2 + z_p^2)^{1/2}} \quad (2)
 \end{aligned}$$

With this equation the average solid angle for a sheet of particles generated immediately above the detector was calculated to be 1.74 sr, and the differential muon flux from [23] could be used in the calculation of the total muon flux for a given level at Homestake mine.

2. Capture Rate for Negative Muons

The stopping muons can be captured by an argon nucleus to generate radioactive isotopes such as ^{40}Cl , etc. There are two sources of stopping muons for a given depth in an underground laboratory: 1) the through-going muons come to the end of their energy range and 2) the secondary muons generated locally by the primary muons and their daughter pions. The capture rate for muons as a function of the depth of the detector can be calculated using the following equation:

$$R_\mu^{\text{capt}} = R_\mu^S \cdot f_{\text{capt}} \cdot f_c \cdot f_{ch} \cdot f_g, \quad (3)$$

where the contributing terms are as follows:

1. R_μ^S is the stopping muon rate (derived below).
2. f_{capt} is the fraction of muons that are captured,

$$f_{\text{capt}} = \frac{\tau_{\text{lifetime}}}{\tau_{\text{capt}}}, \quad (4)$$

with τ_{capt} = muon capture time in argon,

$$\frac{1}{\tau_{\text{capt}}} = \frac{1}{\tau_{\text{lifetime}}} - \frac{1}{\tau_0}, \quad (5)$$

$\tau_{\text{lifetime}} = 537 \pm 32$ ns in argon [24] and τ_0 = lifetime of muons in a vacuum. Here, $f_{\text{capt}} = 0.76$.

3. f_c is the elemental fraction of the target in the compound

$$f_c = \frac{a_i \cdot Z_i}{\sum_i a_i \cdot Z_i}. \quad (6)$$

For the LBNE detector $f_c = 1$.

4. f_{ch} is the charge ratio of negative muons to total muons,

$$f_{ch} = \frac{\mu^-}{\mu^- + \mu^+}. \quad (7)$$

It is 0.44 on the surface, but it is assumed that underground the fraction will be similar.

5. f_g is the fraction of reactions that occur with ^{40}Cl in the ground state. Two fractions are considered: $f_{ga} = 0.0712$ [25] and $f_{gb} = 0.2$ (from the Geant4 simulation).

The stopping muon rate can be calculated with the following formula:

$$R_\mu^S = R_\mu^T \cdot R \cdot f_{\text{scale}} \quad (8)$$

where R_μ^T is the through-going muon rate, R is the ratio of stopping to through-going muons and, f_{scale} , the scale factor, $\frac{\text{mass}}{\text{area}} \frac{1}{100\text{g}\cdot\text{cm}^{-2}}$, scales from a 1 m.w.e detector to a

larger size and was calculated to be 19.5 for the simulated LBNE detector.

The through-going muon rate is defined as

$$R_\mu^T = \phi_\mu^T \cdot \Omega \cdot S_{\text{area}}, \quad (9)$$

where Ω is the solid angle, ϕ_μ^T is the differential through-going muon flux, and S_{area} is the area through which the through-going muons transverse the detector. Using the measured differentiated through-going muon flux from F.E. Gray *et al.* [23] and the average solid angle, the calculated through-going muon rate is 4.2×10^6 per day at 800 ft and 5910 per day at 4850 ft.

Two equations were analyzed for the ratio of stopping to through-going muons. The first,

$$R_1 = \frac{0.3}{< E_\mu >} + 5.7 \cdot 10^{-5} \cdot n_0 \cdot < E_\mu >^{0.7} \quad (10)$$

was proposed by Chudakov *et al.* in Ref. [26] using experimental data, and considers both the through-going portion as well as the muons produced by cascades with $< E_\mu >$ defined as

$$< E_\mu > = \frac{\epsilon_\mu (1 - \exp(-bh))}{\gamma_\mu - 2}, \quad (11)$$

where n_0 varies from 0.4-0.75 depending on depth (here, $n_0 = 0.4$ was used to fit the equation best with simulated data), $\gamma_\mu = 3.77$ [28], $\epsilon_\mu = 693$ GeV, $b = 0.4$ km.w.e, and h is the depth in km.w.e [30]. The second equation considered,

$$R_2 = \gamma_\mu \frac{\Delta E \cdot \exp(\frac{h}{\xi})}{[\exp(\frac{h}{\xi}) - 1] \epsilon_\mu} \quad (12)$$

is a parametrization from [27], where $\gamma_\mu = 3.77$ [30], $\xi = 2.5$ km.w.e., $\Delta E \approx \alpha \Delta x$, $\alpha = 0.268$ GeV/km.w.e. (for $E_\mu \geq 1000$ GeV) and $\Delta x = 100$ g cm $^{-2}$, h is the depth in km.w.e, and $\epsilon_\mu = 618$ GeV [27, 29].

At each depth, two rates were calculated for stopping muons and compared to the simulated values. These can be seen in Table V.

TABLE V: Comparison of calculated stopping muon rates to simulated results.

| Process | Level | |
|-------------------------|--------------------|------|
| | 800 | 4850 |
| $R_{\mu,1}^S$ (per day) | 3.06×10^5 | 251 |
| $R_{\mu,2}^S$ (per day) | 5.45×10^5 | 233 |
| Sim. (per day) | 3.69×10^5 | 173 |

The stopping muon rates are within 30% of the simulated values. The total capture rate of negative muons was calculated using two equations for the ratio of stopping to through-going muons (R_1 and R_2) and the two different ground state fractions (f_{ga} and f_{gb}) resulting in four values (Table VI).

TABLE VI: Comparison of muon capture rates.

| Process | Level | |
|-------------------------------|--------------------|------|
| | 800 | 4850 |
| $R_{\mu,1a}^{capt}$ (per day) | 7286 | 5.97 |
| $R_{\mu,2a}^{capt}$ (per day) | 1.30×10^4 | 5.55 |
| $R_{\mu,1b}^{capt}$ (per day) | 2.05×10^4 | 16.8 |
| $R_{\mu,2b}^{capt}$ (per day) | 3.64×10^4 | 15.6 |
| Sim. (per day) | 2.73×10^4 | 17.5 |

The capture rates and simulated values were plotted as a function of depth (km.w.e) in Fig. 8 using the integrated neutron flux (Eq.(13) Ref. [17]) instead of the differential flux at the specific levels. As it is apparent in Fig. 8, using $R_{\mu,1b}^{capt}$ to calculate the muon capture rate has the best agreement to Monte Carlo.

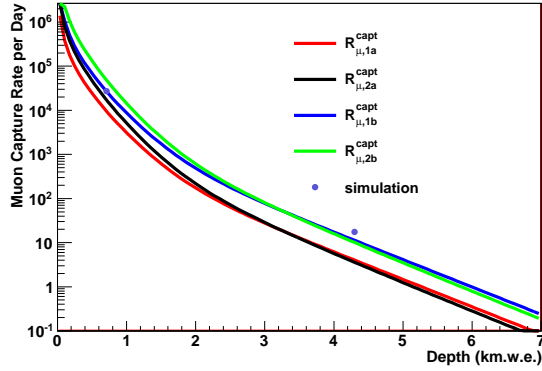


FIG. 8: Capture rates as a function of depth.

3. Production Rate via (n,p) Reaction

Another important reaction that contributes to the production of ^{40}Cl in the detector is the (n,p) reaction, $^{40}\text{Ar}(n,p)^{40}\text{Cl}$. To calculate the production rate the following formula can be used:

$$P_{(n,p)} = \frac{\Phi_n(E_n) \cdot \exp(-\frac{\langle L \rangle}{\lambda_{total}})[1 - \exp(-\frac{\langle L \rangle}{\lambda_{(n,p)}})] \cdot m}{\rho \cdot \langle L \rangle} \quad (13)$$

where m is the mass of the detector, ρ is the density of the detector medium, $\langle L \rangle$ is the average path length, $\Phi_n(E_n)$ is the integrated neutron flux, λ_{total} is the mean free path considering all neutron disappearance reaction channels except (n,p), and $\lambda_{(n,p)}$ is the mean free path of the (n,p) reaction channel.

The first component of the (n,p) production rate, $\Phi_n(E_n) \cdot \exp(-\frac{\langle L \rangle}{\lambda_{total}})$, is the probability that neutrons will survive all reactions except the (n,p) reaction, reducing the flux and availability of neutrons for the production of ^{40}Cl . Similarly, the second term, $[1 -$

$\exp(-\frac{\langle L \rangle}{\lambda_{(n,p)}})]$, is the probability that the remaining neutrons will undergo (n,p) reaction and produce the ^{40}Cl background. The remaining terms, $\frac{m}{\rho \cdot \langle L \rangle}$, are characteristics of the detector.

In calculating the average path length, the angular dependence of the neutrons (and their parent particle muons) was considered using the methodology of Jostlein and McDonald [31]. A $\frac{1}{\cos \theta}$ dependence was used in the calculation.

The mean free path was calculated by

$$\lambda = \frac{A}{\rho \cdot N_a \cdot \sigma} \quad (14)$$

where A is the mass number of the target nucleus, ρ is the density, N_a is Avogadro's number, and σ is the cross section. For the calculation, the flux weighted cross section, $\bar{\sigma}$, was used

$$\bar{\sigma} = \frac{\sum_i \phi_i \cdot \sigma_i}{\sum_i \phi_i}, \quad (15)$$

where flux and cross section of the same energy, i , are summed together. The cross sections from Geant4 were used for this calculation. It is important to use the flux weighted cross sections to calculate the mean free path in order to account for the entire spectrum of possible neutron energies. Unfortunately the Geant4 cross section data does not exceed 100 MeV, however, the calculated values should be accurate to within a factor of two.

Using the above formulas, we have calculated the average path length, the flux weighted cross sections, and the mean free path for neutrons at the levels of 800 ft and 4850 ft. Table VII shows the results. As can be seen in Table VII, the values are similar as anticipated.

TABLE VII: The calculated parameters for Eq. 13.

| Level | Path length $\langle L \rangle$ (cm) | Cross section | | Mean free path | |
|-------|---|----------------------------|----------------------------|------------------------|------------------------|
| | | $\bar{\sigma}_{(n,p)}$ (b) | $\bar{\sigma}_{total}$ (b) | $\lambda_{(n,p)}$ (cm) | λ_{total} (cm) |
| 800 | 572.2 | 0.0209 | 0.181 | 2280 | 262.9 |
| 4850 | 570.8 | 0.0209 | 0.181 | 2280 | 262.9 |

Two main sources of neutrons are considered for both 800 ft and 4850 ft: 1) the muon-induced neutrons entering the detector from the experimental hall (Source I neutrons) and 2) the muon-induced neutrons in the detector when muons pass through the target (Source II neutrons). The final calculated (n,p) production rate for both levels are listed in Table VIII with the relevant neutron flux in the detector above the (n,p) reaction threshold.

As shown in Table VIII, the predicted production rates using the analytic models agree well with the Geant4 simulation.

TABLE VIII: The calculated (n,p) production rates.

| | | $\Phi(E_n)$ (cm ⁻² s ⁻¹) | ⁴⁰ Cl rate per day | |
|-----------|----------|---|-------------------------------|--------|
| Source I | Level | Flux | Analytic models | Geant4 |
| | 800 | 8.8×10^{-7} | 4784 | 3667 |
| | Neutrons | 1.66×10^{-10} | 9.07 | 9.3 |
| Source II | Level | Flux | Analytic models | Geant4 |
| | 800 | 1.4×10^{-6} | 66978 | 40587 |
| | Neutrons | 6.0×10^{-10} | 54 | 54 |

C. Scaling Function

Muon-induced processes and the cosmogenic radioactivity production depends strongly on the target and it must be evaluated individually for the experiment. However, the production rate is proportional to muon flux, or neutron flux, and their interaction cross-section. The energy dependence of the total cross-section for all muon-induced radio-isotopes in the scintillator was evaluated assuming the power law [32]

$$\sigma_{tot}(E_\mu) \propto E_\mu^\alpha, \quad (16)$$

where α varies from 0.50 to 0.93 with a weight mean value $\langle \alpha \rangle = 0.73 \pm 0.10$ [33]. For a given target atoms N and the cross-section σ_0 at the Earth surface where the average muon energy is about 4 GeV, the muon-induced cosmogenic radioactivity (R_{iso}) depends on the differential muon energy spectrum dN_μ/dE_μ at the experimental site at a depth h_0 ,

$$R_{iso} = N\sigma_0 \int_0^\infty \left(\frac{E_\mu}{4 \text{ GeV}}\right)^\alpha \frac{dN_\mu}{dE_\mu} dE_\mu, \quad (17)$$

As a simplification, the production rate is written as a function of the average muon energy $\langle E_\mu \rangle$ at a depth h_0 [33]:

$$R_{iso} = \beta_\alpha N\sigma_{4 \text{ GeV}} \left(\frac{\langle E_\mu \rangle}{4 \text{ GeV}}\right)^\alpha \phi_\mu, \quad (18)$$

where ϕ_μ is the total muon flux at the experimental site and $\beta_{0.73} = 0.87 \pm 0.03$ is the correction factor for the averaging of E_μ [33]. For a given detector target and a depth, the cosmogenic production rate as a function of depth is thus obtained

$$\frac{R_{iso}(unknown)}{R_{iso}(known)} = \left(\frac{E_{\mu,unknown}}{\langle E_{\mu,known} \rangle}\right)^\alpha \frac{\phi_\mu(unknown)}{\phi_\mu(known)}. \quad (19)$$

III. DEPTH-SENSITIVITY RELATION

LBNE is an extremely rich physics program that will measure neutrino properties using a neutrino beam. In addition, LBNE will also measure supernova neutrinos and proton decays. Each of these physics channels has its unique signal region in terms of energy distribution.

For example, measuring the parameters of neutrino oscillation with a neutrino beam has an energy region from 1 to 8 GeV while the energy region of proton decay ranges from 100 to 938 MeV. The signal of supernova neutrinos resides between 5 to 50 MeV. It is difficult to establish a depth-sensitivity relation for all physics channels using a single plot. We elaborate the muon-induced backgrounds for each of physics channels below.

A. Muon and the Muon-induced Neutron Rates

Utilizing the above formulas, the muon and the muon-induced neutron rates as a function of depth can be shown in Fig. 9. It is clear that the event rates decrease rapidly when the depth increases. The fluctuation of muon and the muon-induced neutron rates from seasonal variation can result in backgrounds for all physics channels depending on the depth.

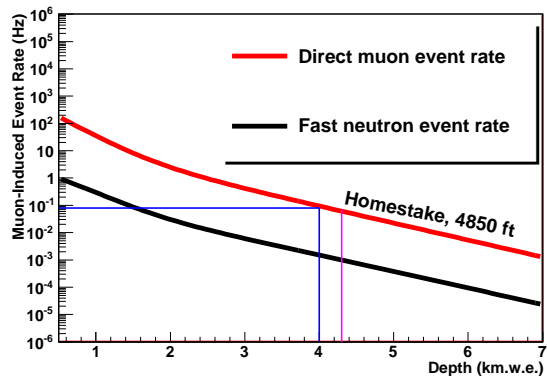


FIG. 9: Muon and muon-induced neutron rates as a function of depth. Shown is for the energy deposition greater than 5 MeV in the detector.

B. Cosmogenic Production Rates

The cosmogenic production rate also decreases with increasing of depth. As an example, Fig. 10 shows the ⁴⁰Cl production rate as a function of depth. The cosmogenic produced radioactive isotopes can be backgrounds for the detection of relic supernova neutrinos.

C. π_0 Production Rates

The neutrino beam-induced natural current and charge current π_0 productions are important backgrounds to the ν_e appearance. However, π_0 can also be produced by muons and muon-induced neutrons in the detector. Fig. 11 shows the energy deposition from π_0 events created by fast neutrons in the detector. It is worth mentioning that there are also multiple π_0 events along the neu-

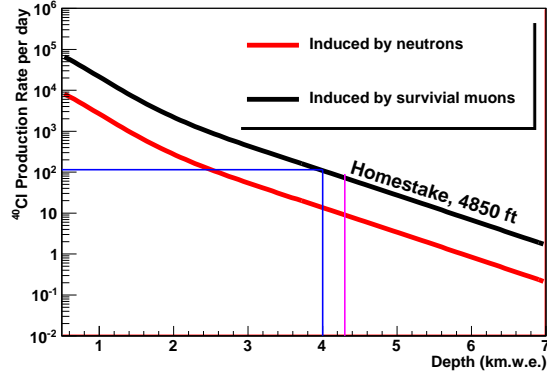


FIG. 10: ^{40}Cl production rates produced by (n,p) reaction as a function of depth.

tron track. The production of π_0 as a function of depth is

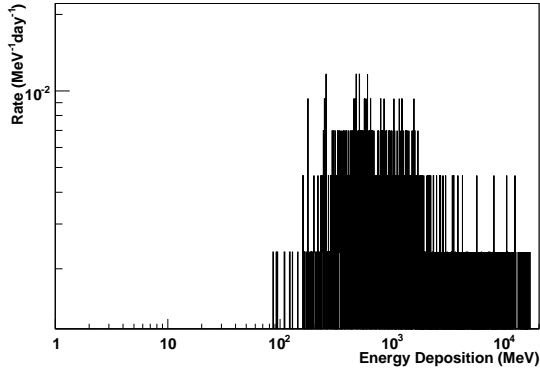


FIG. 11: π_0 events in the detector at the 4850-ft level.

shown in Fig. 12. It is clear that the π_0 produced by fast neutrons entering the detector can be a significant background to the beam physics program. This is because the fluctuation of the π_0 production due to the seasonal variation of muon flux and neutron flux results in a level of 22 π_0 events per year in the detector. In addition, the statistical fluctuation of the π_0 has a similar level of 33 π_0 events. Adding both in quadratic, the level of fluctuation in the production of π_0 can be about 40 events per year. This is significant even at the 4850-ft level. Depending on the capability of discriminating single π_0 events between the beam neutrino-induced and the cosmic neutron-induced, a greater depth (7400-ft level) can be an effective option to further reduce this background.

D. Backgrounds for ν_e Appearance

The ν_e appearance is essential to the measurements of neutrino properties with a neutrino beam. The anticipated signal in a 20 kton LAr detector is about 75 events per year [21]. The muon-induced backgrounds can be

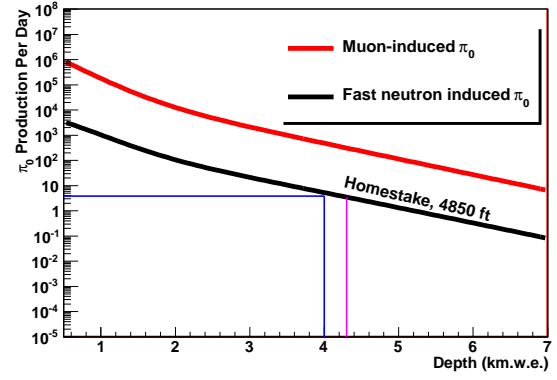


FIG. 12: π_0 production rates as a function of depth.

measured with the beam-off. However, the fluctuation of background events resulting from statistical and seasonal variation is a main source of background. This background as a function of depth is shown in Fig. 13. As can be seen in Fig. 13, the depth must be greater than 4.0 km.w.e. in order to have a reasonable measurement of ν_e appearance at SURF.

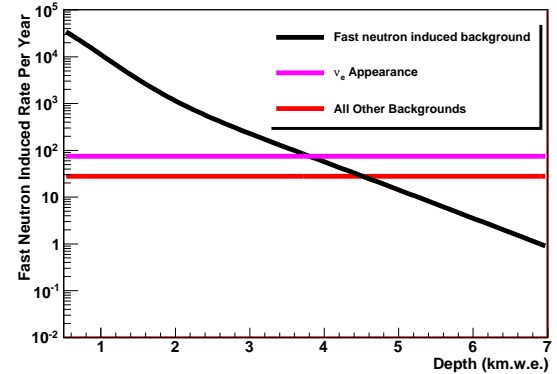


FIG. 13: Muon-induced background as a function of depth. Shown is the average value of statistical fluctuation induced by fast neutrons. Note that signal and the other total backgrounds were estimated using Ref. [21].

IV. CONCLUSION

We evaluate the muon-induced background as a function of depth for a long baseline neutrino experiment with liquid argon as the target at the SURF at Homestake. Both Geant4 simulations and analytic methods are employed in the evaluation of background event rate in the region of interest using the available muon and neutron energy spectra from Ref. [17] and the measured muon flux from Ref. [23]. The muon and muon-induced neutron rates are calculated for the energy greater than 5 MeV.

The cosmogenic processes are discussed in detail for negative muon capture, (n,p), and (p,n) reactions. The dominant backgrounds are from both stopping muons and the high energy neutrons generated by muons in the surrounding materials and in the target. In summary, the background sources are: 1) the negative stopping muon capture; 2) the neutron (n,p), (n,d),(n,t), (n, α), etc; and 3) the muon-induced showers. The cosmogenic production rate as a function of depth is evaluated for negative stopping muon capture and fast neutrons separately. As can be seen from the above discussion, the cosmogenic production rate induced by the muon-induced processes reduces significantly when the depth is larger than 4.0 km.w.e. It is clear from Fig. 8 and Fig. 10, the ^{40}Cl production is less than 100 per day when the depth is greater than 4.0 km.w.e. We conclude the following:

- The 800-ft level is too shallow for a beam-related neutrino physics because the muon rate (~ 88 Hz) is too high. Though LAr TPC is better in identifying π_0 events comparing to a water Cerenkov detector [34], the π_0 produced by muons seen in Fig. 12 can be a significant background.
- The 800-ft level cannot be used to detect supernova neutrinos for a galactic supernova neutrino burst with a time window of 30 seconds at 10 kpc. This is because the expected charge current events in a 20 kton detector used in the simulation from such a burst are about 1300 events [20]. They corresponds to about 44 Hz. However, the total muon-induced rate is about 88 Hz at this level. The signal is immersed in background. In addition, the frequency of galactic supernova occurs at a level of once per 50 years [35].
- The muon-induced processes can be significant background for an argon-based detector in the de-

tection of relic supernova neutrinos with a depth less than 4.0 km.w.e. With a 20 kton detector, we expect less than 30 events per year from relic supernova neutrinos [36]. The relic supernova neutrinos can be detected with the accumulation of the detector lifetime.

- Fig. 13 shows a depth requirement for the ν_e appearance from a neutrino beam. It is clear that a meaningful measurement of CP violation can only be accomplished when the depth is greater than 4.0 km.w.e.
- Finally, positioning a LAr detector near surface, i.e. at NOVA depths, will increase the backgrounds by three orders of magnitude compromising the direct ν program.

Therefore, a depth larger than 4.0 km.w.e. is needed for an argon-based detector. The 4850-ft level at Homestake mine can be an appropriate home for this detector.

V. ACKNOWLEDGEMENT

The authors wish to thank Kevin Lesko, Bob Svoboda, Christina Keller, and Angela A. Chiller for a careful reading of this manuscript. In particular, the authors would like to thank Kevin Lesko for his many invaluable suggestions in presenting various backgrounds clearly in this paper. This work was supported in part by NSF PHY-0758120, DOE grant DE-FG02-10ER46709, the Office of Research at University of South Dakota and a 2010 research center support by the State of South Dakota.

-
- [1] Fukuda Y. *et al.* (Super-Kamiokande Collab.), Phys. Rev. Lett. 1998. V. 81. P. 1562.
 - [2] Ambrosio M. *et al.* (MACRO Collab.), Phys. Lett. B. 2003. V. 566. P. 35.
 - [3] Sanchez M. C. *et al.* (Soudan 2 Collab.), Phys. Rev. D. 2003. V. 68. P. 113004.
 - [4] Aliu E. *et al.* (K2K Collab.), Phys. Rev. Lett. 2005. V. 94. P. 081802.
 - [5] Michael D. G. *et al.* (MINOS Collab.), Phys. Rev. Lett. 2006. V. 97. P. 191801.
 - [6] Ahmad Q. R. *et al.* (SNO Collab.), Phys. Rev. Lett. 2002. V. 89. P. 011301.
 - [7] Cleveland B. T. *et al.* Astrophys. J. 1998. V. 496. P. 505.
 - [8] Hirata K. S. *et al.* (KAMIOKANDE-II Collab.), Phys. Rev. Lett. 1989. V. 63. P. 16.
 - [9] CHOOZ, M. Apollonio *et al.*, Eur. Phys. J. C27 (2003) 331, arXiv:hep-ex/0301017.
 - [10] V. Barger *et al.*, Phys. Rev. D 74, 073004 (2006).
 - [11] P. Adamson *et al.*, MINOS Collaboration, arXiv:1202.2772.
 - [12] K. Abe *et al.*, arXiv:1106.2822v2.
 - [13] Fukugita M. and Yanagida T., Phys. Lett. B. 1986. V. 174. P. 45; Anisimov A., Blanchet S., and Di Bari P., JCAP. 2008. V. 0804. P. 033.
 - [14] Feruglio F., Strumia A., and Vissani F., Nucl. Phys. B. 2002. V. 637. P. 345 (Nucl. Phys. B. Addendum. 2003. V. 659. P. 359).
 - [15] The LBNE Collaboration. LBNE Conceptual Design Report, Volume 5: Liquid Argon Detector for LBNE, Feb. 17, 2012.
 - [16] M. Bass *et al.*, LBNE Collaboration, A Study of the Physics Potential of the Long-Baseline Neutrino Experiment Project with an Extensive Set of Beam, Near Detector and Far Detector Configurations, LBNE-PWG-002, INT-PUB-11-002. V. Barger *et al.*, Report of the US long baseline neutrino experiment study, FERMILAB-0801-AD-E, BNL-77973-2007-IR, May 2007.
 - [17] D.-M. Mei and A.Hime, Phys. Rev. D. 73 (2006) 053004.

- [18] S. Agostinelli *et al.*, Nucl. Instr. and Meth. in Physics Research A 506 (2003) 250-303. J. Allison *et al.*, IEEE Transactions on Nuclear Science 53 No. 1 (2006) 270-278.
- [19] M.S. Gordon *et al.*, IEEE Trans. Nucl. Sci. 51(6) (2004)3427.
- [20] A. Bueno, I. Gil-Botella, A. Rubbia, hep-ph/0307222v1.
- [21] Jon Urheim, Indiana University for the LBNE Science Collaboration, Status of the LBNE Long Baseline Neutrino Experiment, Meetings of the Division of Particles and Fields of the American Physical Society, 9 August 2011.
- [22] H. Gotoh and H. Yagi, Nucl. Instr. and Meth. 96 (1971) 485-486.
- [23] F.E. Gray *et al.*, Nucl. Instr. and Meth. A 638 (2011) 63-66.
- [24] T. Suzuki, D.F. Measday, and J.P. Roalsving, Phys. Rev. C 35 (1987)2212.
- [25] A.V. Kinskikh *et al.* Russ. Acad. Sci (2008) 72 6 735.
- [26] Alekseev, E. N., Chudakov, A. E., Gurentsov, V. A., Mikheev, S. P., Tizengausen, V. A., Proceedings of the 13th International Conference on Cosmic Rays, held in Denver, Colorado, Volume 3 (MN and HE Sessions), p.1936.
- [27] Thomas K. Gaisser, *Cosmic Rays and Particle Physics* (Cambridge University Press, New York, 1990), p. 71.
- [28] P. Lipari and T. Stanev, Phys. Rev. D **44**, 3543 (1991).
- [29] D.E. Groom *et al.* (Particle Data Group), Eur. Phys. J. C. **15**, 1 (2000).
- [30] Donald E. Groom *et al.*, At. Data Nucl. Data Tables **78**, 183 (2001).
- [31] Hans Jostlein and Kirk T. McDonald *Path Length of Muons Traversing an Arbitrary Volume* (2007)
- [32] F.F. Khalchukov, *et al.*, II Nuovo Cimento, **18 C**(5) (1995) 517.
- [33] T. Hagner *et al.*, Astroparticle Physics **14** (2000)33-47.
- [34] Bob Svoboda, Overview of the Long Baseline Neutrino Experiment, INT Program 10-2b, Long-Baseline Neutrino Physics and Astrophysics, July 26-August 27, 2010.
- [35] R. Diehl and C. Winkler, "Integral identifies supernova rate for Milky Way". European Space Agency. 2006-01-04. Retrieved 2007-02-02.
- [36] A.G. Cocco, *et al.*, JCAP12(2004)002 doi:10.1088/1475-7516/2004/12/002.